Available online at www.sciencedirect.com

ScienceDirect

Journal of Magnesium and Alloys 10 (2022) 1598–1608

www.elsevier.com/locate/jma

Full Length Article

Different role of second phase in the micro-galvanic corrosion of WE43 Mg alloy in NaCl and Na_2SO_4 solution

Baojing Feng[a,b], Guonan Liu[a,b], Peixu Yang[a,b], Sensen Huang[c], Dongqing Qi[d], Peng Chen[e], Chengduo Wang[a,b], Jiang Du[a,b], Shaojun Zhang[a,b], Jinhui Liu[a,b,*]

[a] *Henan Province Industrial Technology Research Institute of Resources and Materials, Zhengzhou University, Zhengzhou, 450001, China*
[b] *School of Materials Science and Engineering, Zhengzhou University, Zhengzhou, 450001, China*
[c] *Institute of Metal Research, Chinese Academy of Sciences, Shenyang, 110016, China*
[d] *School of Chemistry and Chemical Engineering, Shandong University, Jinan, 250100, China*
[e] *Department of Materials Science and Engineering, Texas A&M University, College Station, TX, 77843, USA*

Received 11 August 2020; received in revised form 31 October 2020; accepted 16 December 2020
Available online 23 February 2021

Abstract

Effect of the second phase in the micro-galvanic corrosion of a commercial Mg alloy containing rare earth elements, cast WE43 alloy, was investigated in 0.6 M NaCl solution and 0.6 M Na_2SO_4 solution by scanning electron microscopy (SEM) observations, scanning Kelvin probe force microscopy (SKPFM) analysis, hydrogen evolution, weight loss measurement, and electrochemical techniques. It is confirmed that the second phase of cast WE43 alloy is more active than Mg matrix and exhibits an anodic role in the micro-galvanic corrosion with α-Mg matrix as cathode and dissolves preferentially in Na_2SO_4 solution, in contrast to the situation in NaCl solution. The corrosion rate of cast WE43 alloy in Na_2SO_4 solution is much higher than that in NaCl solution, which is different from the conventional wisdom and could be attributed to the different role of the second phase in the micro-galvanic corrosion in two solutions.

Keywords: Mg rare earth alloy; Second phase; Micro-galvanic corrosion; Anode role; Solution anion.

1. Introduction

Magnesium alloys are widely used in automotive, aircraft, and aerospace industries [1–5] for their benefits of low density, high specific strength [6] and good biocompatibility [7], thermally conductive [8], and electromagnetic shield ability. However, poor corrosion resistance and low absolute strength performance severely restrict their widespread application [9–11]. By adding rare earth elements, Mg alloy improves its high temperature creep resistance and strength and corrosion resistance [3,12]. For the WE43 alloy (Mg-4Y-3Gd-1Nd-0.5Zr), the addition of Y, Gd, and Nd elements improves its fire resistance and mechanical properties (i.e. tensile strength and creep) at ambient and high temperature [12]. Normally, it is known that the corrosion resistance of Mg alloy is closely related to the surface film and the micro-galvanic corrosion between second phase and Mg matrix [13–16]. The addition of RE elements could improve the protection of the surface film and weak the micro-galvanic corrosion between the second phase and Mg matrix [17–21].

Generally, it is believed that the activity of the second phase is lower than that of the magnesium matrix, not only the traditional Mg alloys such as Mg-Al and Mg-Zn systems [16,19,22], but also the Mg rare earth alloys [2,15]. Liu et al. [15] studied the binary Mg-Re alloys and found that the second phases of Mg-Re alloys exhibit higher electrode potential than that of the α-Mg matrix phase and act as the cathode in the micro-galvanic corrosion in simulated body fluid. Feng et al. [2] found a cathode role of the $Mg_{41}Sm_5$ phase in

* Corresponding author at: Henan Province Industrial Technology Research Institute of Resources and Materials, Zhengzhou University, No.100 Science Avenue, Zhengzhou, China.
E-mail address: liujinhui@zzu.edu.cn (J. Liu).

https://doi.org/10.1016/j.jma.2020.12.013

mitigating localized corrosion of Mg-Sm-Zn-Zr alloy in NaCl solution. Such nobler second phases will accelerate the dissolution of the α-Mg matrix in the micro-galvanic corrosion [23–25]. However, some researchers reported that the second phase is more active than the α-Mg matrix and acts as the anode of micro-galvanic corrosion in Mg rare earth alloys. Liu et al. [26] found that the potential of second phases in cast EW75 (Mg-5Y-7Gd-1Nd-0.5Zr) is more negative than the α-Mg matrix and preferentially dissolved by SKPFM analysis and immersion measurement. Cai et al. [27] indicated both the $Mg_{60}Zn_{32}Nd_8$ phase and the $Mg_{35}Zn_{40}Nd_{25}$ phase have a similar Volta potential which is approximately 400 mV less than the α-Mg matrix, which acted as the micro-anodes in micro-galvanic corrosion. As summarized above, researchers hold different opinions about the role of the second phase in the micro-galvanic corrosion of the Mg rare earth alloys.

Considering the application scenarios, Mg rare earth alloys were immersed in corresponding solutions to simulate the real environment, such as seawater [15] mainly containing NaCl, simulated body fluid [27] (Cl^-, SO_4^{2-}, HPO_4^{3-} and HCO_3^-), and atmospheric environments [28] (Cl^- and SO_4^{2-}). Nevertheless, the relationship between anions in the solution and galvanic corrosion mechanisms of Mg alloy is rarely involved. Combining the literature research data and our early experiments, it is worth investigating the effect of anions on micro-galvanic corrosion.

In our present work, the corrosion behavior of WE43 alloy in Na_2SO_4 and NaCl solution was investigated to clarify the effect of solution anions on the micro-galvanic corrosion and corrosion resistance.

2. Experimental methods

2.1. Materials and solution

Cast WE43 alloy ingot was kindly supplied by Yueyang Yuhua Metallurgical New Materials Co., Ltd., and used as a raw material in this work. Its nominal composition is 1.55 wt.% Gd, 3.79 wt.% Y, 2.43 wt.% Nd, 0.5 wt.% Zr and Mg balance, which is in accordance with ASTM B951–11. Specimens with dimensions of $10\times10\times10$ mm^3 were cut from the cast ingot by wire cutting, followed by sanding the surface impurities and grinding the corrosion observation surface with water through successive grades of SiC abrasive papers from P120 to P5000 grit prior to the following measurement.

The immersion test was conducted in 0.6 M Na_2SO_4 and 0.6 M NaCl solution which were prepared at room temperature (25 °C ± 0.5) by dissolving Na_2SO_4 or NaCl in distilled water. The reagents were provided by Shanghai Aladdin Biochemical Technology Co. Ltd. All reagents and deionized water used in this work were A.R. grade, and all experiments were performed at least three times.

2.2. Microstructural characterization

The transversal section of the specimens was polished with 1 μm diamond at 1000 rpm through the polishing machine-YMP-2A produced by Shanghai Metallographic Machinery Co., Ltd.; and then they were rinsed with deionized water, degreased with absolute ethanol, and dried in compressed cold air.

Microstructure and elements distribution of the surface were investigated by Field emission scanning electron microscopy (SEM; American FEI Quanta 250 FEG) equipped with energy-dispersive spectrometry (EDS) with an acceleration voltage of 20 kV.

Volta potential distributions were probed using a Scanning Kelvin Probe Force Microscope (SKPFM; Dimension Icon, Bruker Nano Inc.) in work function mode. The probe used in SKPFM measurements was magnetic etched silicon probe (MESP) ($k = 2.8$ N/m, Bruker Nano Inc., CA, USA) with piezoelectric tube size of $125\times125\times5$ μm. The results were analyzed by Nano-Scope Analysis software.

2.3. Immersion measurements

The specimens used in immersion testing were the same as that of microstructure characterization. Before immersion, WE43 alloy specimens were polished to obtain a bright surface. And then, specimens for corrosion morphology observation were exposed to 0.6 M NaCl solution and 0.6 M Na_2SO_4 solution at 25 °C ± 0.5 for 10 min, 30 min, 2 h, 10 h, 24 h, and 7 days, respectively. After immersion, all specimens were rinsed with deionized water, degreased with ethanol, and dried in cold airflow. The immersed specimens were immersed in a chromic acid solution containing 180 g/L CrO_3 for 5 min to remove the corrosion products at room temperature. The corrosion surface after removing corrosion products and the cross-section morphology of corroded samples after 7 days of immersion in 0.6 M NaCl solution and 0.6 M Na_2SO_4 solution were observed by SEM-BSE and EDS.

The surface film cross-section morphology of cast WE43 alloy immersed in 0.6 M NaCl and Na_2SO_4 solution for 24 h with the corrosion products not removed were observed by SEM-BSE.

Hydrogen gas was collected in a burette through a funnel mounted over a specimen with dimensions of $30\times30\times10$ mm^3 in a beaker containing 2 L of testing solution. The sample was hung by a thread so that it did not touch the beaker to avoid crevice corrosion [29]. At the same time, specimens for weight loss measurements were weighed before exposure using a digital balance-JA3003 produced by Shanghai Precision Instrument Co., Ltd. with a precision of 0.0001 g as the original weight. After immersion in 0.6 M NaCl solution and 0.6 M Na_2SO_4 solution at 25 °C ± 0.5 for 7 days respectively, specimens were immersed in the solution of 180 g/L CrO_3 for 10 min, then washed with deionized water, degreased with ethanol, and dried by cold air, followed by being weighed to gain the weight loss.

2.4. Electrochemical measurements

All electrochemical tests were conducted in 0.6 M NaCl solution or 0.6 M Na_2SO_4 solution using a CHI660D

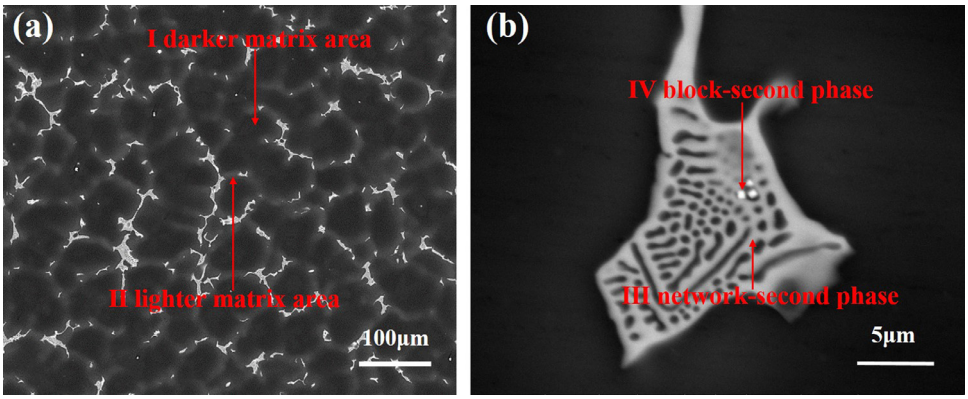

Fig. 1. BSE-SEM morphologies on the surface of WE43 alloy.

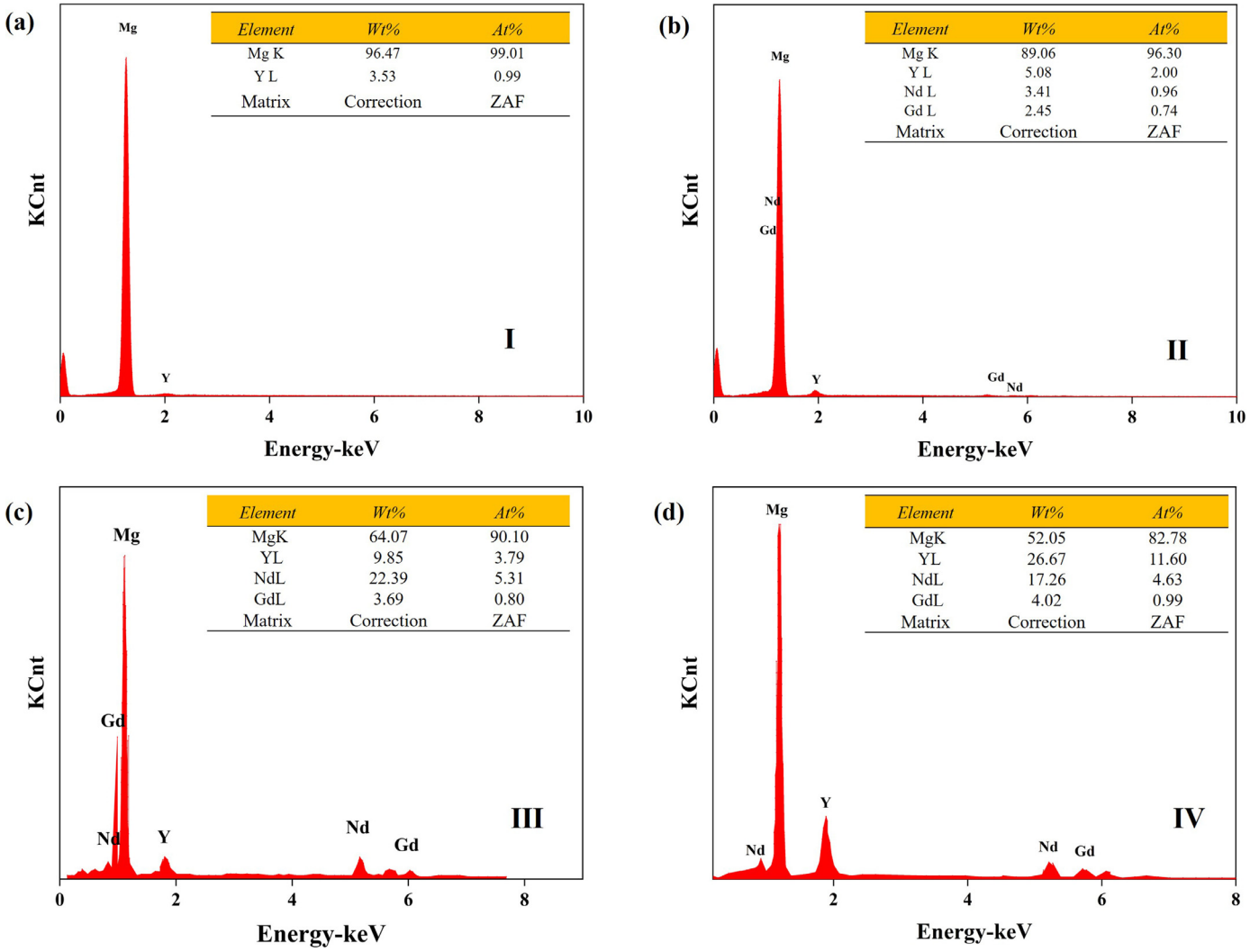

Fig. 2. EDS quantitative analysis of areas and points marked in Fig. 1.

electrochemical workstation through a standard three electrodes configuration with platinum as the counter electrode, an R232 saturated calomel electrode (SCE) (+0.242 V vs. standard hydrogen electrode (SHE)) as the reference electrode, and the samples, sealed in epoxy resin with an exposed area of 1 cm^2, as the working electrode.

The open-circuit potential (OCP) was measured for all samples at least 30 min. The cathodic polarization curves were started at the OCP value and terminated at a potential of −250 mV vs. OCP. The anodic polarization curves were started at the OCP value and terminated at a final current density of 1 mA cm^{-2}. The scan rate was 0.5 mV s^{-1}.

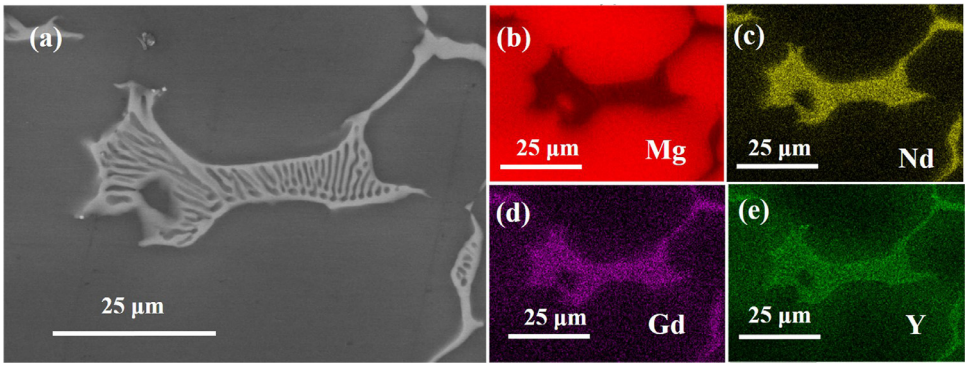

Fig. 3. High magnification BSE-SEM morphology and EDS mapping of the network-shaped second phase: (a) Surface morphology; EDS mapping of (b) Mg, (c) Nd, (d) Gd and (e) Y.

Prior to measurement, the working electrode was stabilized for about 5 min. The corrosion current density was fitted by cathodic curves. The electrochemical impedance spectroscopy (EIS) immersion time were 2, 13, 16 and 24 h in 0.6 M NaCl solution and 0.6 M Na_2SO_4 solution, respectively. The parameters of EIS were set AC voltage disturbance and frequency ranged. The AC voltage disturbance and frequency ranged were 5 mV and 100 kHz to 0.01 Hz. The EIS spectra were fitted using the ZSimpWin 3.20 software.

All electrochemical measurements were carried out at 25 °C ± 0.5 and replicated at least three times to ensure reproducibility.

3. Results

3.1. Microstructural characterization of WE43 alloys

The surface morphology of cast WE43 alloy is shown in Fig. 1. The Mg matrix is composed of two parts which exhibit a darker area (marked I) and a lighter area (marked II). The EDS of darker matrix area is shown in Fig. 2a, and the lighter adjacent to the grain boundaries in the absence of second phases indicates RE enrichment, which is consistent with the EDS result in Fig. 2b. The shiny part is the second phase, and they are discretely precipitated around grain boundaries. It can be observed that the dendritic intermetallic phases are composed of two kinds of second phases in the form of the network-shaped (marked III) and the block-shaped (marked IV), and the blocked-shaped second phase is discretely distributed around the network-shaped one. The chemical composition of two kinds of second phases is shown in 2c and 2d The network-shaped second phase contains 90.10%Mg, 3.78%Y, 5.31%Nd, and 0.80%Gd (At.), which should be the $Mg_{45}Nd(Gd)_5$ and Mg_5Gd [20]. The block-shaped second phase in cast WE43 alloy consists of 82.78%Mg, 11.60%Y, 4.63%Nd, and 0.99%Gd (At.), which should be the $Mg_{24}Y_5$ and $Mg_{41}Nd_5$ [30]. The volume fraction of the network-shaped second phase is much larger than that of the block-shaped second phase, thus this thesis mainly researches the role of the network-shaped second phase in the micro-galvanic corrosion. Fig. 3 shows the high magnification morphology of the network-shaped second phase and corresponding EDS mapping, which indicates the distribution of Mg, Y, Gd, and Nd. In addition, see Fig. 3d and e, there are also some rare earth elements in the matrix around the second phase, which is in accordance with the results of area II.

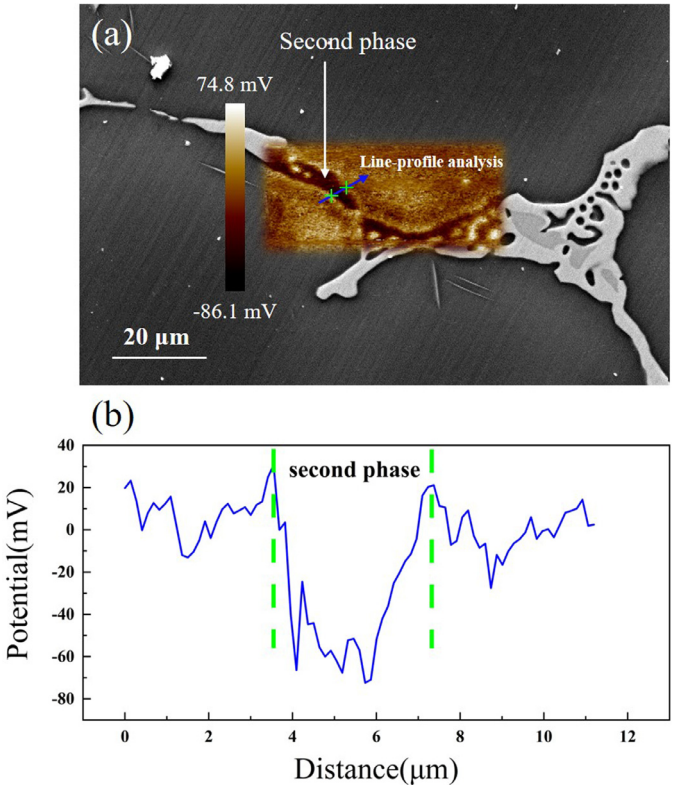

Fig. 4. SKPFM results of cast WE43: (a) surface Volt potential map, and (b) line-profile analysis of relative Volta potential through second phase.

3.2. Scanning Kelvin probe force microscopy analysis

Volte potential distribution of cast WE43 alloy is shown in Fig. 4. The second phase shows a darker color than the surrounding Mg matrix in Fig. 4a. Under the work function mode of SKPFM, the bright areas correspond to the more positive potential, while the dark areas correspond to the more

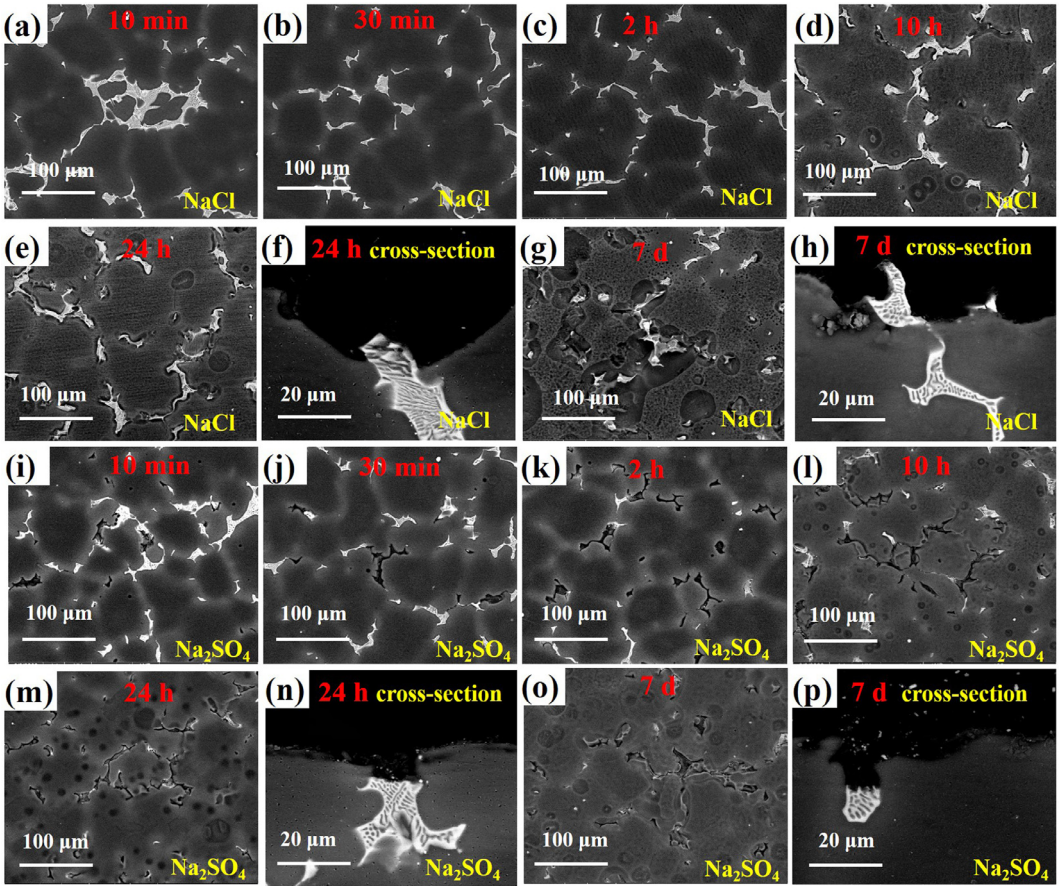

Fig. 5. The corrosion morphologies and cross-section morphologies of WE43 alloy in NaCl for (a) 10 min, (b) 30 min, (c) 2 h, (d) 10 h, (e, f) 24 h, (g, h) 7 d and in Na_2SO_4 solution for (i) 10 min, (j) 30 min, (k) 2 h, (l) 10 h, (m, n) 24 h, (o, p) 7 d with corrosion product removed.

negative potential. It indicates that the second phase is more active than Mg matrix. From the corresponding Volte potential of the line-profile in Fig. 4b, the Volte potential difference between the second phase and Mg matrix is 80 mV approximately. Base on this result, the second phases may act as micro-anodes to corrode preferentially.

3.3. Immersion tests

3.3.1. Corrosion morphology characterization

The corrosion morphologies of cast WE43 alloy specimens immersed in 0.6 M NaCl solution and 0.6 M Na_2SO_4 solution for different time intervals with corrosion products removed are shown in Fig. 5. In NaCl solution, weak corrosion of Mg matrix of cast WE43 alloy could be observed in the surface morphologies during the initial immersion intervals shown in Fig. 5a, b, c, meanwhile, the second phase keeps undamaged. When it comes to 10 and 24 h (Fig. 5d and e), the matrix around the second phase has been eroded severely. According to the cross-section morphology immersed for 24 h in Fig. 5f, the second phase protrudes approximately 5 μm from the surrounding matrix. After immersion for 7 days in Fig. 5g and h, the matrix around the second phase is damaged badly and the protruding length increases to 17 μm. Comparing to the corrosion morphologies of WE43 alloy in NaCl solution, there is a big difference of that in Na_2SO_4 solution. In Fig. 5i, the second phase of WE43 alloy is attacked preferentially for 10 min immersion in Na_2SO_4 solution, while the matrix keeps intact whether the darker or the lighter areas. Fig. 5j and k show that the dissolution of the second phase expands when immersed for 30 min and 2 h. With the immersion time increasing, the second phase dissolution proceeds, meanwhile, pit corrosion appears in the darker matrix area (Fig. 5l) and the corrosion degree turns more severe after immersion for 24 h shown in Fig. 5m. More fundamentally, it is shown in the cross-section morphology (Fig. 5n) that the depth of the second phase dissolution is about 7 μm for 24 h immersion. After 7 days of immersion, no second phase could be observed from the surface morphology shown in Fig. 5o, and the depth of the second phase dissolution increases to about 15 μm, see the cross-section morphology in Fig. 5p. On the other side, it could be observed in Fig. 4o that the lighter matrix area along grain boundaries dissolved obviously.

Fig. 6 shows the high magnification microscopic morphology of the second phase in WE43 alloy immersed in two different solutions for 7 days. In the NaCl solution, the Mg matrix around the second phase dissolves, while the second phase is left as the cathode, which is shown in Fig. 6a. The EDS results in Fig. 6d prove that the residual rod-like parts are eutectic α-Mg matrix, which indicates the anodic role of

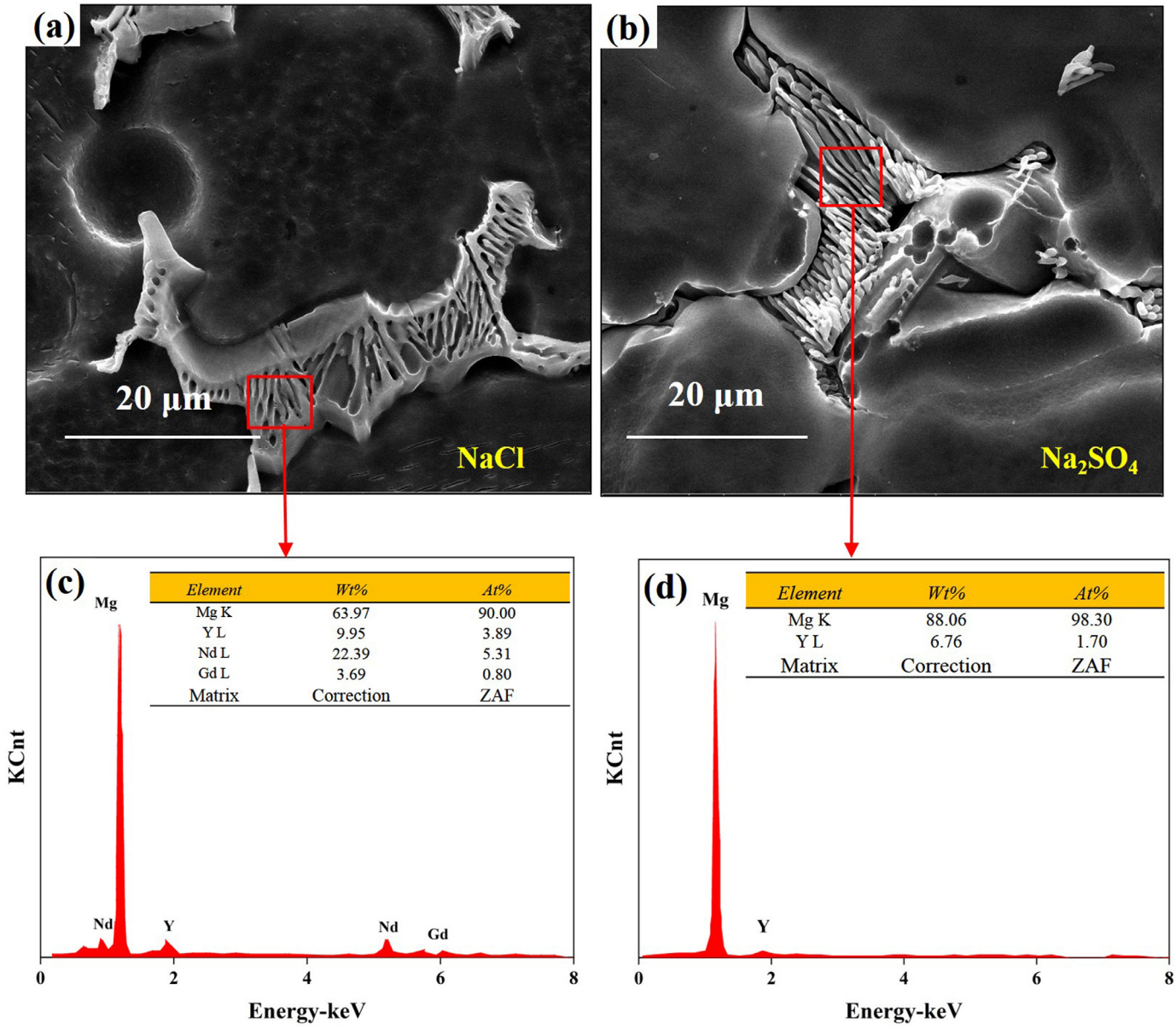

Fig. 6. High magnification SEM and corresponding EDS of corrosion morphologies of WE43 alloy in (a) NaCl solution and (b) Na_2SO_4 solution for 7 d.

the second phase in the micro-galvanic corrosion when WE43 alloy immersed in Na_2SO_4 solution.

3.3.2. Surface film characterization

The cross-section morphologies of surface film, cast WE43 alloy immersed in 0.6 M NaCl and 0.6 M Na_2SO_4 solution for 24 h without immersion in chromic acid solution, are shown in Fig. 7. In NaCl solution, the cathodic second phase was covered by the homogeneous precipitation of $Mg(OH)_2$, with the thickness about 2 μm. In Na_2SO_4 solution, however, no protective surface film was found on the upper of the second phase, which indicates that rare earth elements dissolve in Na_2SO_4 solution, without rare earth oxide or hydroxide precipitation formed. Meanwhile, this result clarifies the misunderstanding of the chromic acid, since some researches attribute the dissolution of second phase to the attack of chromic acid [31-33].

Table 1
Weight loss rates of cast WE43 alloy after immersion in the different solution for 7 days (mm $year^{-1}$).

Mass loss rate (mm $year^{-1}$)	Sample 1	Sample 2	Sample 3	Average
0.6 M NaCl solution	0.5669	0.4892	0.7946	0.6169
0.6 M Na_2SO_4 solution	1.4823	1.2771	1.0728	1.2774

3.3.3. Gravimetric results

The weight loss rate of cast WE43 alloy after immersed in 0.6 M NaCl and Na_2SO_4 solution for 7 days is shown in Fig. 8 and corresponding data is listed in Table 1. The

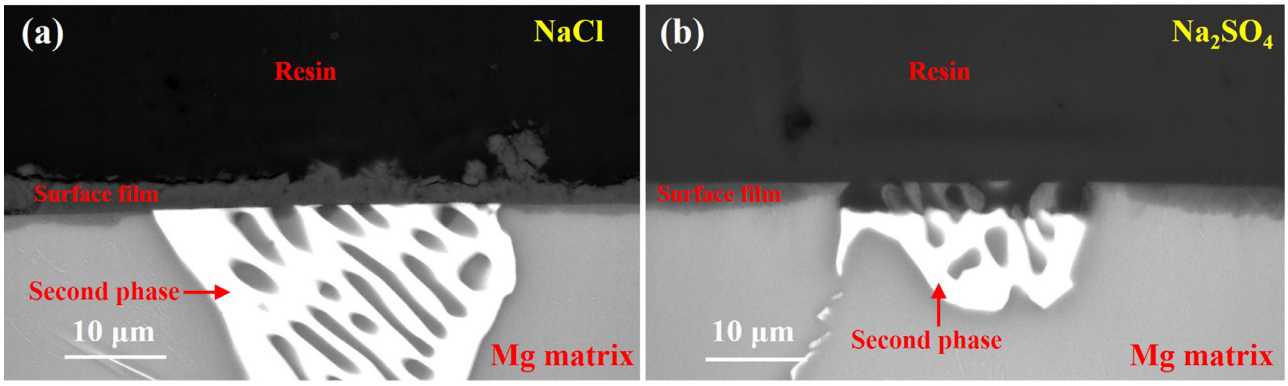

Fig. 7. Surface film cross-section morphologies of cast WE43 alloy immersed in 0.6 M NaCl and Na_2SO_4 solution for 24 h.

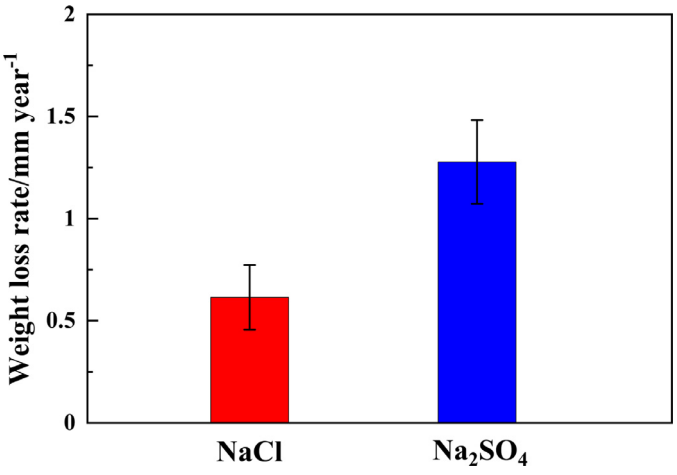

Fig. 8. Weight loss rates of cast WE43 alloy after immersion in 0.6 M NaCl solution and Na_2SO_4 solution for 7 d.

weight loss rate of cast WE43 alloy in Na_2SO_4 solution is about double that in NaCl solution during the whole immersion measurement, implying that cast WE43 alloy suffered more serious corrosion damage in the Na_2SO_4 solution.

3.3.4. Hydrogen evolution results

The hydrogen evolution amount and hydrogen evolution rates with an immersion time of WE43 alloy in 0.6 M NaCl solution and 0.6 M Na_2SO_4 solution are shown in Fig. 9, respectively. WE43 alloy in Na_2SO_4 solution exhibits a larger hydrogen evolution amount and faster hydrogen evolution rate than that in NaCl solution, which coincides with the results of weight loss.

3.4. Electrochemical corrosion behavior of Mg alloy WE43

3.4.1. EIS analysis

Fig. 10 shows the EIS plots of cast WE43 alloy after immersed for 2, 13, 16, and 24 h, respectively. All plots consist of a high-frequency capacitance loop followed by a medium frequency capacitance loop and a low-frequency inductance loop. The high-frequency capacitance loop can be associated with the electric double layer at the interface of the Mg substrate and electrolyte. The medium frequency capacitance loop should be related to the surface oxide film. The short low-frequency inductance loop should be attributed to the initiation of localized corrosion.

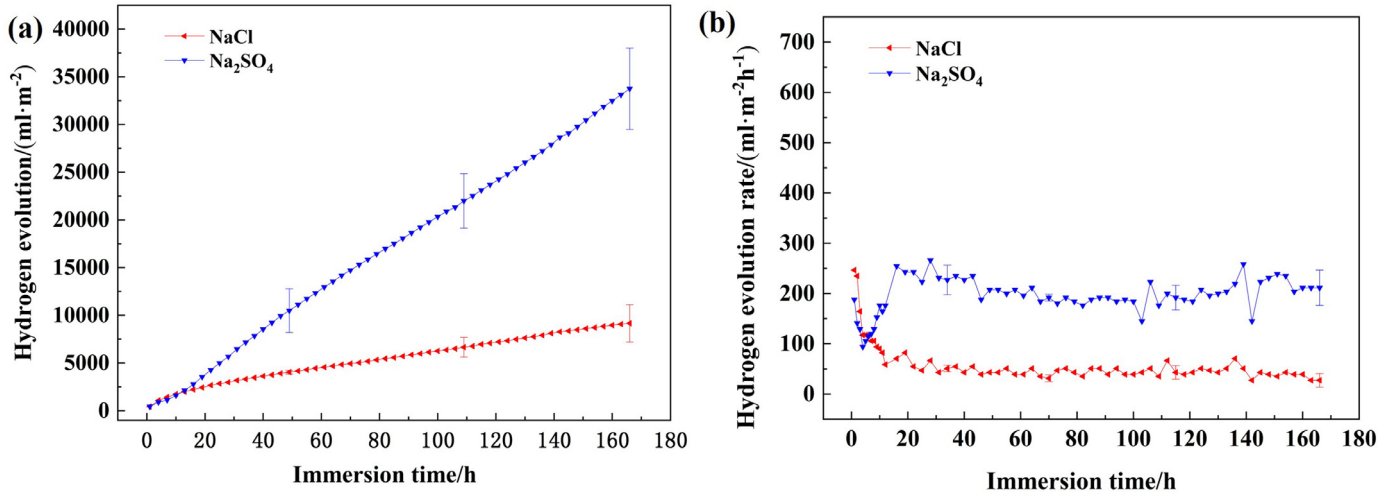

Fig. 9. Hydrogen evolution amount and rate of WE43 alloy in 0.6 M NaCl solution and Na_2SO_4 solution, respectively.

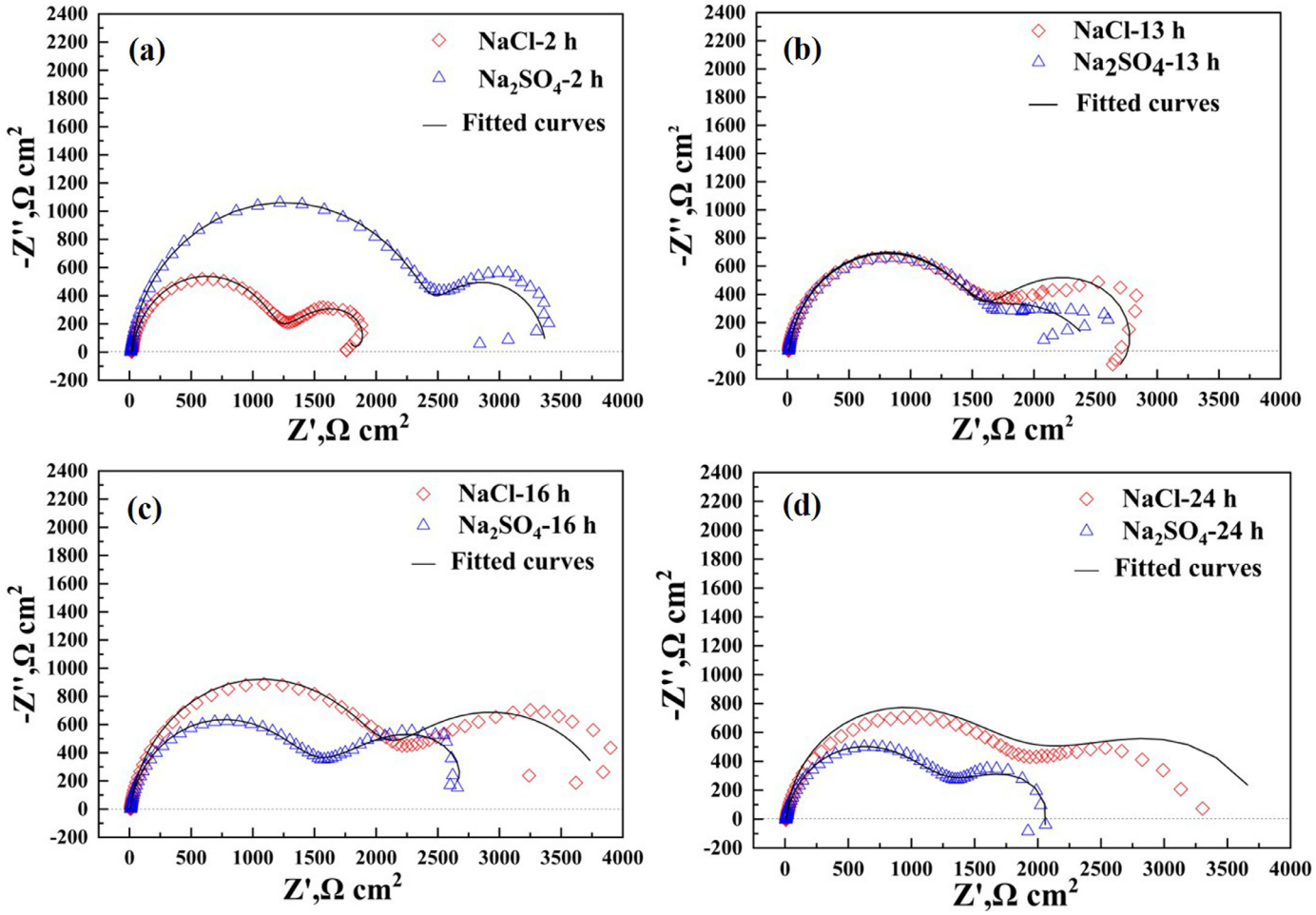

Fig. 10. The Nyquist plots of WE43 alloy immersed in 0.6 M Na_2SO_4 solution and NaCl solution for 2, 13, 16, 24 h, respectively.

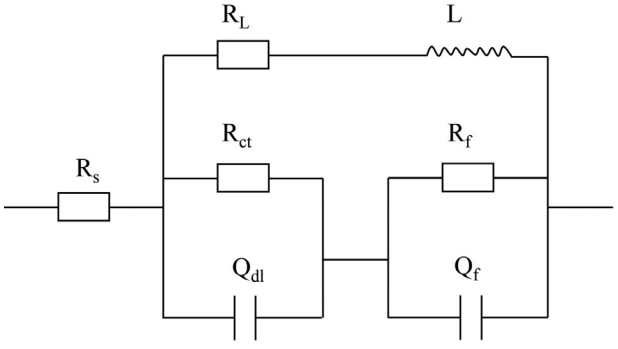

Fig. 11. Equivalent circuit applied in the fitting of experimental data of WE43 alloy immersed in: (a) Na_2SO_4 solution, (b) NaCl solution.

EIS spectra are fitted using the equivalent circuits as shown in Fig. 11. Fitting results are listed in Table 2. In the proposed equivalent circuits, R_s is the solution resistance. R_t is the charge transfer resistance, and Q_{ld} is related to the capacity of the electric double layer. R_t and Q_{ld} together describe the first capacitance loop in high frequency. R_f and Q_f represent the surface film resistance and capacity, respectively. They are used to describe the second capacitance loop in medium frequency. L is the inductance of the electrochemical reactions at the film-substrate interface; R_L is the resistance of the inductance. R_L and L are used to describe the low-frequency inductance loop. The capacitive reactance radian in NaCl solution increases with the immersed time increasing, while in Na_2SO_4 solution, the capacitive reactance arc decreases with immersion time increasing, which means cast WE43 alloy suffers from severe corrosion in Na_2SO_4 solution.

3.4.2. Potential dynamic polarization curves

The cathodic polarization curves and anodic polarization curves of cast WE43 alloy immersed in 0.6 M NaCl solution and 0.6 M Na_2SO_4 solution are shown in Fig. 12. The cathodic side of the polarization curve is controlled by hydrogen evolution reaction while the anodic branches in the polarization curves represent the anodic dissolution of Mg alloy, and the polarization test is usually applied to study the corrosion mechanism of alloy in the initial corrosion stage. According to the fitting results shown in Table 3, the E_{corr}

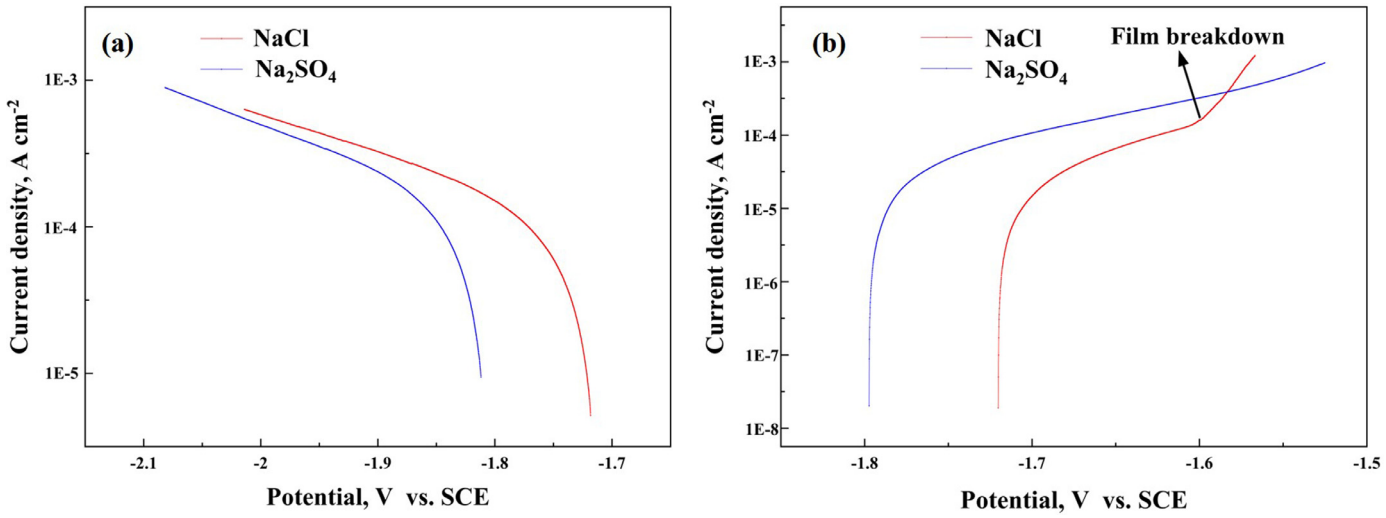

Fig. 12. Comparison of polarization curves of WE43 alloy in 0.6 M NaCl solution and Na_2SO_4 solution, respectively. (a) cathodic side, (b) anodic side.

Table 2
Fitting results of EIS spectra.

		R_s	Q_{dl}	n_{dl}	R_{ct}	Q_f	n_f	R_f	L	R_L
2 h	Na_2SO_4	9.245	0.000731	0.8096	1531	0.001128	0.9668	2068	0.75	1.12
	NaCl	18.78	1.27E-05	0.9452	1111	0.002172	0.9279	1643	2.69	279
13 h	Na_2SO_4	10.16	0.000179	0.9266	1404	0.000986	0.8326	1075	4.14	8.64
	NaCl	10.62	0.001296	0.8931	1987	1.66E-05	0.9242	1480	1.57	8065
16 h	Na_2SO_4	9.839	2.08E-05	0.9076	1404	0.000126	0.8295	1509	0.56	8.15
	NaCl	8.997	1.47E-05	0.9187	1835	0.000342	0.8429	2180	1994	3888
24 h	Na_2SO_4	6.625	2.01E-05	0.8985	1167	0.001347	0.8595	968.2	2.68	0.061
	NaCl	5.992	0.000893	0.7969	1763	1.53E-05	0.9416	1730	2204	1.28

Table 3
The fitting result of the cathode polarization curve.

Solution	$E_{corr}(V_{SCE})$	$i_{corr}(\mu A\ cm^{-2})$	$b_c(mV\ decade^{-1})$
NaCl	-1.72 ± 0.02	65.7 ± 2	86.7 ± 2
Na_2SO_4	-1.80 ± 0.03	46.9 ± 3	80.6 ± 2

of WE43 alloy in NaCl and Na_2SO_4 solution are -1.72 and -1.80 V_{SCE}, and the i_{corr} are 65.7 and 46.9 $\mu A\ cm^{-2}$, respectively. As a consequence, the cast WE43 alloy in NaCl solution exhibits a higher activity and faster corrosion rate than that in Na_2SO_4 solution in the initial corrosion stage, which is in accordance with the results of hydrogen evolution results shown in Fig. 9 and the initial results of Nyquist plots in Fig. 10.

In the anodic sides, the curves of WE43 alloy in NaCl solution showed an obvious breakdown potential (-1.60 V_{SCE}). Before the breakdown potential, WE43 showed a significant passivation effect, which is related to the protective effect of the film. In Na_2SO_4 solution, however, the cast WE43 alloy is always in active dissolution, which indicates the surface film of WE43 alloy in Na_2SO_4 solution is non-protective corresponding to the cross-section morphologies of surface film shown in Fig. 7.

4. Discussion

4.1. Different micro-galvanic corrosion behavior

On the basis of the above results, the second phase of WE43 Mg Alloy shows a different role in the micro-galvanic corrosion in NaCl solution and Na_2SO_4 solution, which means the micro-galvanic corrosion between the second phase and Mg matrix of WE43 alloy has a close relationship with the solution anions.

The high magnification of WE43 alloy immersed in NaCl solution and Na_2SO_4 solution for 7 days, Fig. 6, presents the details of micro-galvanic corrosion behavior. In NaCl solution, the Mg matrix dissolves preferentially and acts as the anode in the micro-galvanic corrosion couple with the second phase as the cathode. It is interesting that the etch pit around the second phase in NaCl solution happens to be the residual part in the Na_2SO_4 solution, which is direct evidence that the second phase plays a different role in the micro-galvanic corrosion of WE43 Mg alloy in two solutions.

In NaCl solution, the micro-galvanic corrosion between the matrix and the second phase is not obvious at the early corrosion stage. With immersion time increasing, the dissolution of the matrix around the second phase becomes clearer.

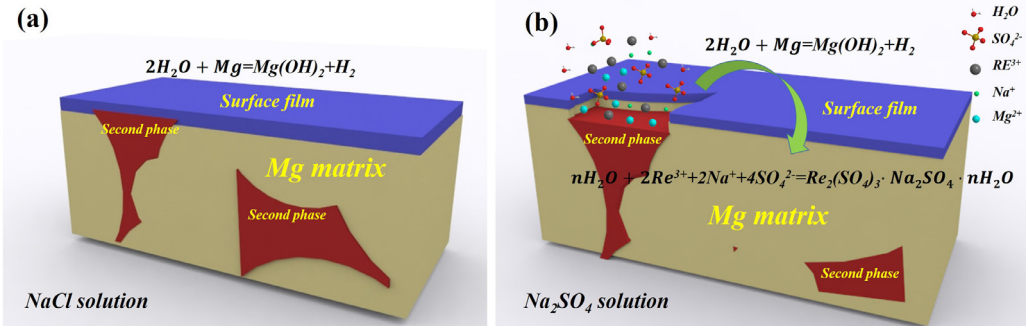

Fig. 13. Corrosion mechanism diagram. (a) WE43 alloy immersed in NaCl solution, (b) WE43 alloy immersed in Na_2SO_4 solution.

Although corrosion pots in the matrix area can be observed, micro-galvanic corrosion between the second phase and matrix dominates the process, which is observed in Fig. 5a-h. The corrosion progress of WE43 alloy in Na_2SO_4 solution is quite different from that in NaCl solution. In the Na_2SO_4 solution, corrosion progress can be divided into three stages. In the first stage, the second phase is attacked preferentially and acts as the anode in the micro-galvanic corrosion with the matrix protected as the cathode. The corrosion area of the second phase expands at the surface with immersion time increasing, seen in Fig. 5i, j, and k. In the second stage, most of the second phase has disappeared at the surface morphology and they continue dissolving straight down with the adjacent lighter matrix area protected, meanwhile, pit corrosion occurs in the darker matrix area. Micro-galvanic corrosion between the second phase and the lighter matrix area and dissolution of the darker matrix area occur simultaneously, which is observed in Fig. 5l, m, and n. In the third stage, as the depth of second phase dissolution reaches the extreme value and the micro-galvanic corrosion between the second phase and matrix weaken, dissolution of the lighter matrix area initiates due to the RE enrichment in comparison with the darker matrix area, which can be seen in Fig. 5o and p. As for the phenomenon that the second phase acts as micro-anode in micro-galvanic corrosion of cast WE43 alloy immersed in Na_2SO_4 solution, there are two hypotheses: I SO_4^{2-} is capable to couple with rare earth elements, which conduce the dissolution of second phase and formation of a complex compound bonding with coordinated bond [34]; II a film consisting of rare earth oxide and hydroxide covers the second phase, however, this film could be attacked readily in Na_2SO_4 solution and lose the protective effect [31]. The schematic description of the micro-galvanic corrosion of WE43 alloy in NaCl solution and Na_2SO_4 solution is shown in Fig. 13.

The ionic concentration of 0.6 M Na_2SO_4 solution is 1.5 times that of 0.6 M NaCl solution. In order to eliminate the influence of this factor, the immersion experiment in 0.3 M Na_2SO_4 solution was then re-run. As shown in the following Fig. 14, the second phase still acts as micro-anode in the micro-galvanic corrosion and dissolved preferentially.

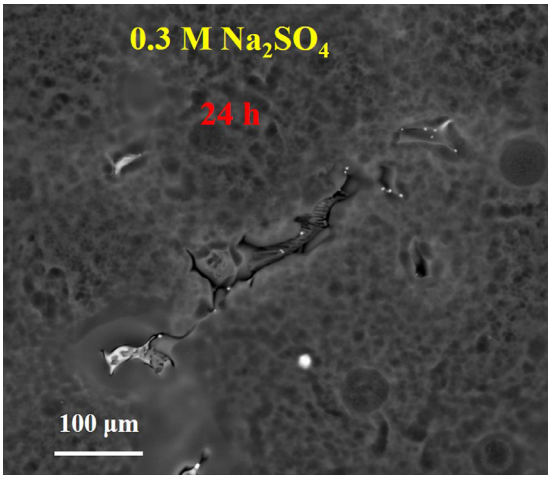

Fig. 14. The corrosion morphologies of WE43 alloy in Na_2SO_4 solution for 24 h.

4.2. Comparison of corrosion resistance of cast WE43 in NaCl solution and Na_2SO_4 solution

In this research, WE43 alloy shows better corrosion resistance in NaCl solution comparing to that in Na_2SO_4 solution, which is different from the conventional wisdom [35]. From the weight loss results in Fig. 8 and Table 1, the corrosion rate of WE43 alloy immersed in Na_2SO_4 solution for 7 days is double that in NaCl solution, which is the most intuitive characterization of corrosion resistance. Hydrogen evolution and weight loss occur simultaneously, and the hydrogen evolution rate is a more detailed demonstration of corrosion rate with immersion time [1]. In Fig. 9, WE43 alloy in Na_2SO_4 solution expresses a faster hydrogen evolution rate than that in NaCl solution. The hydrogen evolution rate of WE43 alloy immersed in Na_2SO_4 solution is about six times that in NaCl solution. From the polarization curves, a significant passivation effect can be observed in NaCl solution, which is related to the protective effect of the film. In Na_2SO_4 solution, the anodic polarization curve indicates the cast WE43 alloy is always in active dissolution, which could be related to the absence of protective film on the upper of second phase.

The corrosion resistance of Mg alloy could be mainly comprehended form two aspects, micro-galvanic corrosion and surface film: "large cathodic area-small anodic area" could cause a severe damage in galvanic corrosion, the WE43 alloy in Na_2SO_4 solution corresponds to which exactly; the surface film of WE43 alloy in NaCl solution is much more protective than that in Na_2SO_4 solution. Thus, the corrosion rate of WE43 alloy in Na_2SO_4 solution is much higher than that in NaCl solution.

5. Conclusion

(1) The immersion and electrochemical tests demonstrate that the second phases of cast WE43 act as micro-anodes in the micro-galvanic corrosion in Na_2SO_4 solution, which is greatly different from the situation in NaCl solution.
(2) No protective film on the second phase of cast WE43 alloy in Na_2SO_4 solution and the corrosion rate in Na_2SO_4 solution is much higher than that in NaCl solution, which conflicts with the traditional impression.

Acknowledgments

This work was funded by the National Key Research and Development Program of China (Grant No. 2016YFB0301001 and 2016YFB0301101), Major Projects for Collaborative Innovation of Zhengzhou (Grant No.18XTZX12010), and Certificate of Postdoctoral Research Grant in Henan Province (Grant No. 201903011).

References

[1] A.D. King, N. Birbilis, J.R. Scully, Electrochim. Acta. 121 (2014) 394–406, doi:10.1016/j.electacta.2013.12.124.
[2] Y. Feng, L. Wei, X. Chen, M. Li, Y. Cheng, Q. Li, Corros. Sci. 159 (2019) 108133, doi:10.1016/j.corsci.2019.108133.
[3] F. Czerwinski, Corros. Sci. (2014), doi:10.1016/j.corsci.2014.04.047.
[4] S. Li, A.C. Bacco, N. Birbilis, H. Cong, Eval. Program Plann. 112 (2016) 596–610, doi:10.1016/j.corsci.2016.08.022.
[5] Y. Yang, X. Peng, H. Wen, Mater. Sci. Eng. A. (2014), doi:10.1016/j.msea.2014.05.064.
[6] J. Zhang, L. Zhang, Z. Leng, S. Liu, M. Zhang, Scr. Mater. 68 (2013) 675–678, doi:10.1016/j.scriptamat.2013.01.023.
[7] Z.Z. Yin, W.C. Qi, R.C. Zeng, X.B. Chen, C.D. Gu, S.K. Guan, Y.F. Zheng, J. Magnes. Alloy. 8 (2020) 42–65, doi:10.1016/j.jma.2019.09.008.
[8] S. Li, X. Yang, J. Hou, W. Du, J. Magnes. Alloy. (2020), doi:10.1016/j.jma.2019.08.002.
[9] T. Zheng, Y. Hu, F. Pan, Y. Zhang, A. Tang, J. Magnes. Alloy. 7 (2019) 193–202, doi:10.1016/j.jma.2019.05.006.
[10] T. Xu, Y. Yang, X. Peng, J. Song, F. Pan, J. Magnes. Alloy. 7 (2019) 536–544, doi:10.1016/j.jma.2019.08.001.
[11] S.C. V, R. Dumpala, A.K. S, K. Vv, R.S. B, J. Magnes. Alloy. 6 (2018) 52–58, doi:10.1016/j.jma.2017.12.001.
[12] C. Liu, S. Lu, Y. Fu, H. Zhang, Eval. Program Plann (2015), doi:10.1016/j.corsci.2015.07.020.
[13] M.P. Brady, G. Rother, L.M. Anovitz, K.C. Littrell, K.A. Unocic, H.H. Elsentriecy, G.-.L. Song, J.K. Thomson, N.C. Gallego, B. Davis, J. Electrochem. Soc. 162 (2015) C140–C149, doi:10.1149/2.0171504jes.
[14] P.F. Ye J, X. Chen, J. Li, C. Liu, B. Wu, Vacuum (2020), doi:10.1016/j.vacuum.2020.109629.
[15] J. Liu, D. Bian, Y. Zheng, X. Chu, Y. Lin, M. Wang, Z. Lin, M. Li, Y. Zhang, S. Guan, Acta Biomater 102 (2020) 508–528, doi:10.1016/j.actbio.2019.11.013.
[16] S. Li, X. Yang, J. Hou, W. Du, J. Magnes. Alloy. 8 (2020) 78–90, doi:10.1016/j.jma.2019.08.002.
[17] X. Yu, B. Jiang, J. He, B. Liu, F. Pan, J. Alloys Compd. 749 (2018) 1054–1062, doi:10.1016/j.jallcom.2018.03.342.
[18] Z. Yin, Y. Chen, H. Yan, G. hua Zhou, X. quan Wu, Z. Hu, J. Alloys Compd. 783 (2019) 877–885, doi:10.1016/j.jallcom.2019.01.002.
[19] R. Arrabal, E. Matykina, A. Pardo, M.C. Merino, K. Paucar, M. Mohedano, P. Casajús, Corros. Sci. 55 (2012) 351–362, doi:10.1016/j.corsci.2011.10.038.
[20] S. Leleu, B. Rives, J. Bour, N. Causse, N. Pébère, Electrochim. Acta. 290 (2018) 586–594, doi:10.1016/j.electacta.2018.08.093.
[21] R. Pinto, M.G.S. Ferreira, M.J. Carmezim, M.F. Montemor, Electrochim. Acta. 55 (2010) 2482–2489, doi:10.1016/j.electacta.2009.12.012.
[22] M. Esmaily, J.E. Svensson, S. Fajardo, N. Birbilis, G.S. Frankel, S. Virtanen, R. Arrabal, S. Thomas, L.G. Johansson, Prog. Mater. Sci. 89 (2017) 92–193, doi:10.1016/j.pmatsci.2017.04.011.
[23] Z.P. Cano, J.R. Kish, J.R. Mcdermid, J. Electrochem. Soc. 163 (2016) 62–68, doi:10.1149/2.0151603jes.
[24] G. Galicia, N. Pébère, B. Tribollet, V. Vivier, Corros. Sci. 51 (2009) 1789–1794, doi:10.1016/j.corsci.2009.05.005.
[25] S. Mathieu, C. Rapin, J. Steinmetz, P. Steinmetz, Corros. Sci. 45 (2003) 2741–2755, doi:10.1016/S0010-938X(03)00109-4.
[26] J. Liu, Y. Song, J. Chen, P. Chen, D. Shan, E.H. Han, Electrochim. Acta. 189 (2016) 190–195, doi:10.1016/j.electacta.2015.12.075.
[27] C. Cai, R. Song, L. Wang, J. Li, Appl. Surf. Sci. 462 (2018) 243–254, doi:10.1016/j.apsusc.2018.08.107.
[28] H. Wan, Y. Cai, D. Song, T. Li, Ocean Eng (2019) 106760, doi:10.1016/j.oceaneng.2019.106760.
[29] J. Liu, Y. Song, D. Shan, E.-.H. Han, J. Electrochem. Soc. 163 (2016) C856–C863, doi:10.1149/2.0481614jes.
[30] C. Liu, X. Zhu, T. Zhou, Magnesium Alloy Phase Atlas, Central South University Press, 2006 (In Chinese).
[31] A. Srinivasan, C. Blawert, Y. Huang, C.L. Mendis, K.U. Kainer, N. Hort, J. Magnes. Alloy. (2014) 245–256, doi:10.1016/j.jma.2014.08.002.
[32] W.C. Neil, M. Forsyth, P.C. Howlett, C.R. Hutchinson, B.R.W. Hintonc, Corros. Sci. (2011) 3299–3308, doi:10.1016/j.corsci.2011.06.005.
[33] W.C. Neil, M. Forsyth, P.C. Howlett, C.R. Hutchinson, B.R.W. Hintonc, Corros. Sci. (2009) 387–394, doi:10.1016/j.corsci.2008.11.005.
[34] L. Luo, Rare Met. Cem. Carbides. 43 (2015) 06–0012-04 (In Chinese).
[35] F. Zucchi, V. Grassi, A. Frignani, C. Monticelli, G. Trabanelli, J. Appl. Electrochem. (2006) 195–204, doi:10.1007/s10800-005-9053-3.